

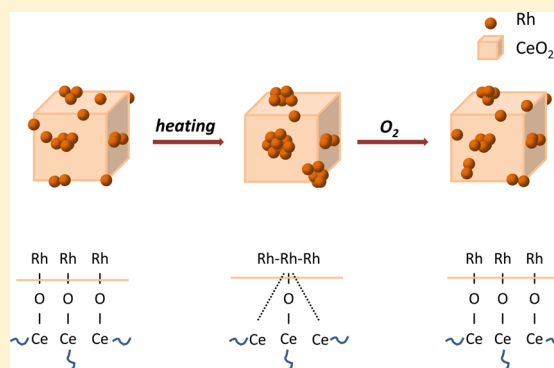
Stability and Temperature-Induced Agglomeration of Rh Nanoparticles Supported by CeO₂

Erika Varga,[†] Péter Pusztai,[‡] Albert Oszkó,[†] Kornélia Baán,[†] András Erdőhelyi,[†] Zoltán Kónya,^{*,‡,§} and János Kiss^{*,†,§}

[†]Department of Physical Chemistry and Materials Science, [‡]Department of Applied and Environmental Chemistry, and [§]MTA-SZTE Reaction Kinetics and Surface Chemistry Research Group, University of Szeged, H-6720 Szeged, Hungary

Supporting Information

ABSTRACT: The effects of reduction by H₂ and by heat treatment in vacuum and in O₂ flow on Rh particle size changes of Rh/CeO₂ samples were studied by X-ray photoelectron spectroscopy (XPS), high-resolution electron microscopy (HRTEM), and CO adsorption followed by diffuse reflectance infrared spectroscopy (DRIFTS). Low-temperature (373–423 K) reduction of Rh without agglomeration is demonstrated. An average particle size of 2.3 ± 1.1 nm was measured by HRTEM regardless of the metal loading (1–5%). On Rh/CeO₂, a significant particle size increase of the Rh particles was detected on heating (773 K). In this work, we suggest that the temperature-induced surface decrease resulting from the sintering of Rh is favored only for well-dispersed particles. XP spectra revealed that the mobile oxygens of CeO₂ fundamentally determine the oxidation state of the supported metals. At elevated temperature, the oxidation of the reduced support surface as well as the metal component takes place because of the segregation of ceria oxygens. When the aggregated particles were reoxidized, the redispersion of Rh was observed probably because of the formation of Rh–O–Ce bonds.



1. INTRODUCTION

Highly dispersed metal nanoparticles are attracting increasing amounts of attention in the catalysis and surface science communities as a result of their unusual physical–chemical properties. In heterogeneous catalysis, it is a well-known phenomenon that the state and the structure of a catalyst can be drastically altered during the catalytic reaction, and in many cases, the real catalyst is formed by the effects of the reacting system. Catalysts used in several commercial chemical processes consist of nanoparticles, usually in the 1–10 nm size range. In many cases, the size and composition of the active site determine the activity of the catalyst and the reaction path.^{1–6} Supported metals such as rhodium may undergo coalescence and various morphological changes during preparation, heat treatment, and reduction. Although in general the pretreatment of the catalysts is carried out at elevated temperature inducing sintering of the noble metal, in most cases this heating procedure is not necessary to obtain fully reduced noble metals. On the other hand, when the support degrades under heating (e.g., titanate nanostructures),^{7,8} low-temperature pretreatment methods are required. In several low-temperature reactions including CO₂ hydrogenation^{9,10} and certain photoinduced catalytic processes,^{11,13} the particle size plays an important role, so the high-temperature reduction step of the metal oxide, which may lead to sintering, should be avoided. Therefore, the detailed investigation of morphological

changes during the reduction and heat treatment is very important in many catalytic systems.

Rhodium supported on CeO₂ is a very active catalyst in several reactions. The best catalysts for the simultaneous reduction of NO and the oxidation of CO and hydrocarbons contain mainly Pt, Pd, and Rh as active components; however, other species, including ceria, are also added to enhance the catalytic performance.^{14,15} It was reported that Rh/ceria is an excellent water–gas shift catalyst.^{16,17} Furthermore, it was revealed that ceria-supported Rh was a promising catalyst for carrying out the steam reforming of ethanol^{18–23} and methane.²⁴ Until now, in efforts to elucidate how interactions between CeO₂ and Rh affect the catalytic performance, several research groups have used surface science tools to study the reactivity of real and well-defined model systems.^{15,25–30} Recently, it was found that the Rh + Co/ceria system was an excellent catalyst for the ethanol steam reforming (ESR) reaction. The addition of a small amount of Rh as a promoter to the Co/CeO₂ catalyst resulted in a significant further increase in the hydrogen selectivity.^{21,22} At the same time, attention is paid to the oxygen reservoir property of CeO₂.^{31,32} Several hypotheses have been put forward, including electron transfer from ceria to Rh particles, structural variation in the Rh

Received: December 8, 2015

Revised: February 22, 2016

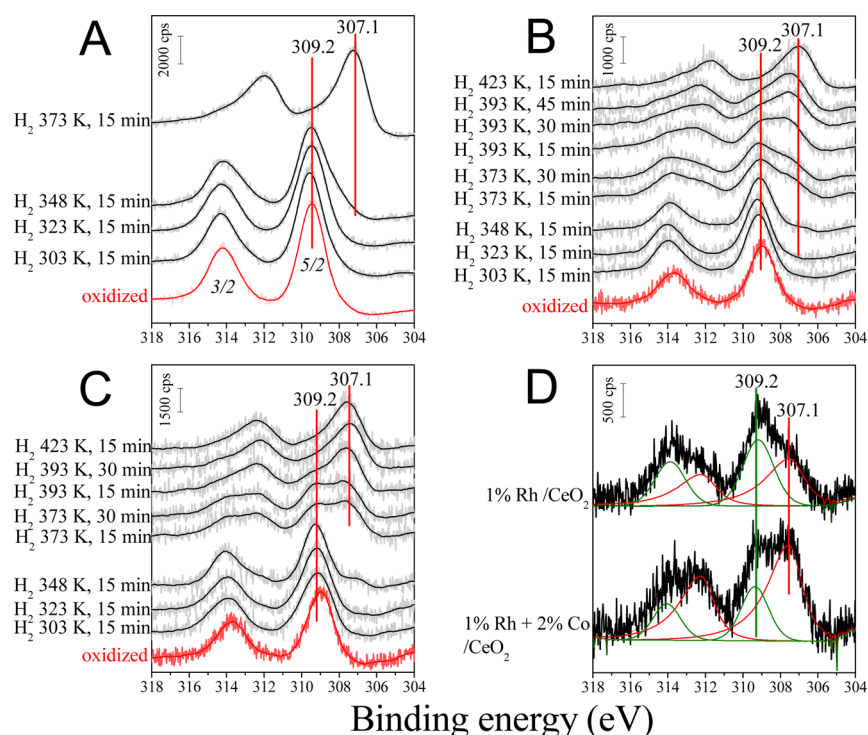


Figure 1. Rh 3d spectra during stepwise reduction for 5% Rh/CeO₂ (A), 1% Rh/CeO₂ (B), and 1% Rh + 2% Co/CeO₂ (C). (D) Comparative figure of 1% Rh/CeO₂ with and without 2% Co, after reduction at 373 K for 15 min.

particles, and oxygen spillover from Rh to ceria.²⁸ Low-temperature oxygen migration from ceria to Rh was also proposed in the ceria–rhodium interaction; in addition, the Rh–O–Ce bond could be formed.^{15,27,29,30} HRTEM images and XP spectra showed significant agglomeration without encapsulation on our Rh/CeO₂ samples, up to 773 K.³³

In the work presented here, we have focused on the morphological changes of Rh during the preparation process. The application of impregnated samples instead of model systems makes it possible to obtain Rh species with oxidation states between 0 and +3. We demonstrate the sintering of reduced Rh under reduction and heat treatment. In order to avoid the formation of large Rh particles during reduction, we describe the low-temperature reduction process of Rh. After that, the changes upon subsequent thermal treatment and reoxidation are presented. We also demonstrate the stabilization effect of cobalt ad-species on Rh particle size on the ceria support during heat treatment.

2. EXPERIMENTAL PROCEDURE

To acquire information on the effect of the quantity of Rh and the Co addition, three samples were prepared: 1% Rh/CeO₂, 1% Rh + 2% Co/CeO₂, and 5% Rh/CeO₂. The catalyst support (CeO₂, Alfa Aesar, 43 m²/g powder) was first calcined at 973 K, then it was impregnated with aqueous solutions of RhCl₃·3H₂O (Johnson Matthey) to yield a nominal metal content of 1 or 5 wt %, and finally, the catalysts were dried at 383 K. For the 1% Rh + 2% Co/CeO₂ catalyst, CeO₂ was impregnated with an aqueous solution of Co(NO₃)₂ for up to 2 wt % Co content and was calcined at 973 K. Subsequently, the same sample was impregnated with the RhCl₃·3H₂O solution and was dried at 383 K. The powders were pressed into pellets. Before measurements, they were oxidized at 673 K in flowing O₂ for 20 min.

XP spectra were taken on a SPECS instrument equipped with a PHOIBOS 150 MCD 9 hemispherical electron energy analyzer using Al K α radiation ($h\nu = 1486.6$ eV). The X-ray gun was operated at 210 W (14 kV, 15 mA). The analyzer was operated in FAT mode with the

pass energy set to 20 eV. For data acquisition and evaluation, the manufacturer's software (SpecsLab2) and commercial (CasaXPS, Origin) software were used. The binding-energy scale was corrected by fixing the Ce 3d u'' peak to 916.6 eV (Figure S1).³⁴ For spectrum deconvolution, the "Curved" named background (supplied by the CasaXPS software), the general Gaussian–Lorentzian (30–70) line shape, and the original asymmetric Rh 3d line shape were used. The Ce³⁺/(Ce³⁺ + Ce⁴⁺) ratio was calculated on the basis of Zhang et al.³⁵

For XPS studies, the powder samples were pressed into pellets of ca. 1 cm diameter and a few tenths of a millimeter in thickness. Sample treatments were carried out in a high-pressure cell connected to the analysis chamber via a gate valve. After the different steps of the experiments, the samples were cooled to room temperature in flowing nitrogen. Then, the high-pressure cell was evacuated, and the sample was transferred to the analysis chamber under high vacuum (i.e., without contact with air), where the XP spectra were recorded. As the next step, the sample was moved back into the catalytic chamber, where it was heated to the desired temperature under N₂, and then the gas flow was changed to H₂ or O₂. Nitrogen was not applied in the agglomeration studies.

The same samples were used for XPS measurements throughout the experiments. During the low-temperature reduction, the sample was reduced for 15 min at the desired temperature that was increased stepwise between two cycles (low-temperature reduction). Agglomeration studies in vacuum were carried out in the 10^{−8} mbar pressure range at 773 K for 1 or 2 h (heating), followed by oxygen treatment at 673 K for 30 or 60 min (reoxidation). In a separate experiment, fresh samples were reduced at 773 K for 1 h (high-temperature reduction).

The morphology of ceria and metal-modified ceria was characterized by transmission electron microscopy (FEI Tecnai G² 20 X-Twin; 200 kV operation voltage, magnification 180 000 \times , 125 pm/pixel resolution). The metal particle size distribution was determined using ImageJ software. At least five representative images of equal magnification taken at different spots on the TEM grid were subjected to rolling ball background subtraction and contrast enhancement, and then the diameter of the metal nanoparticles was measured against the calibrated TEM scale bar. Each diameter distribution histogram was constructed from 200 individual nanoparticle diameter measurements.

DRIFT spectra were recorded using an Agilent CARY-670 FTS-135 FT-IR spectrometer equipped with a diffuse reflectance attachment (Harrick) with BaF₂ windows. Typically, 256 scans were registered at a spectral resolution of 2 cm⁻¹. All spectra were recorded at 293 K. The whole optical path was purged with N₂ from liquid N₂.

3. RESULTS AND DISCUSSION

3.1. Low-Temperature Reduction. In our previous work, it was demonstrated that after 1 h of reduction at 773 K a significant Rh 3d intensity decrease was observed by XPS (Figure S2) and was due to the increase in Rh particle size verified by TEM.³³ At this point, a stepwise temperature-dependent reduction experiment was started to find the lowest temperature for the complete reduction of Rh, which has not yet been done in the literature. Even after oxidation, easily detectable Cl 2p and 2s signals contributed to the survey spectra, and the Rh 3d spectra did not change significantly compared to those of the as-received state (the 5/2 component was located at 309.2 eV). This indicates that Rh is in an oxychloride or hydroxychloride form. However, it cannot be excluded that some Cl migrates to the support, forming Ce^{III}-oxychloride.^{36,38} By the end of treatments in H₂, the residual Cl was removed.

As depicted in Figure 1A, no reduction took place for 5% Rh/CeO₂ up to 323 K; however, when the temperature was raised to 348 K, an asymmetric Rh 3d spectrum could be detected with a shoulder at lower binding energies. After H₂ treatment at 373 K for 15 min, the Rh content was in the metallic state in full as proven by the binding energy (307.1 eV for the 5/2 component) and the characteristic line shape of Rh⁰.

At lower Rh content (1%), the experiment was longer because after treatment at 348 K the Rh 3d spectrum was still very similar to that detected in the oxidized state (Figure 1B). Although significant reduction took place at 373 K in the first 15 min, no further change could be detected after longer H₂ treatment at the same temperature. Upon reduction at 393 K for 30 or 45 min, almost all of the Rh content became metallic; nevertheless, the temperature was set to 423 K to make sure that the reduction was complete.

The same experiment was carried out with 1% Rh + 2% Co/CeO₂ (Figure 1C). On the basis of the XPS results, it can be concluded that the presence of a Co additive enhanced the reduction of Rh. Similar to the Co-free case, 373 K was the lowest temperature for unambiguously starting the reduction. However, it went further on this sample as the Rh⁰ (%) peak area increased compared to the total Rh content (it was 73% instead of 51%, Figure 1D). TPR results on oxide-supported Rh catalysts generally show the opposite trend, (i.e., the maximum in the H₂ consumption is at higher temperature when Co or another transition metal is added³⁹). This difference in reducibility was explained either by the difference in dispersion^{40,41} or the enrichment of the Rh surface in the promoters.^{42,43} On the other hand, it can be concluded from the present results that a long duration treatment at a temperature between the threshold temperature and the TPR peak maximum is sufficient only to reduce a certain amount of Rh. To reduce more metal, the temperature must be increased. These observations suggest a stepwise mechanism, which has a significant temperature dependence; however, as shown by this XPS study, the time effect is not negligible either.

No change in the Rh 3d peak area occurred up to the total reduction for any of the catalysts; this is one of the conclusions

of the XPS experiments. These experimental results indicate that significant agglomeration does not occur during low-temperature reduction, as also supported by FTIR studies.

The corresponding curves in Figure 2 show the CO absorption bands over 1 and 5% Rh/CeO₂ samples after low-

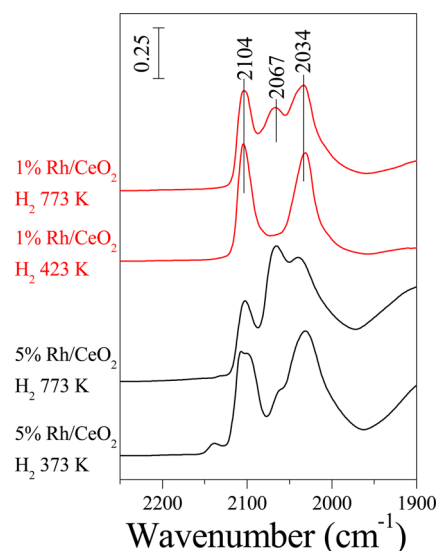


Figure 2. FTIR spectra after CO adsorption over 1 and 5% Rh/CeO₂ after low- (423, 373 K) and high-temperature (773 K) reduction.

temperature reduction. Over the 1% Rh/CeO₂ sample, the exclusive adsorption of gem-dicarbonyl species (2034 and 2104 cm⁻¹) is demonstrated, proving the presence of highly dispersed particles.^{44,46} Over the 5% Rh/CeO₂ sample, an additional weaker band at 2067 cm⁻¹ also emerged as a result of the linear adsorption mode corresponding to some larger particles, but twin bonding was predominant. The signal at 2140 cm⁻¹ is assigned to a minor number of unreduced Rh³⁺ ions.⁴⁷ When these samples were reduced at 773 K for an hour, the proportion of the linearly bonded species increased significantly in both cases as a result of the increased Rh particle size.

3.2. Temperature-Induced Sintering. After the stepwise reduction experiments, the sintering of metallic Rh and its reversibility were studied in detail. The samples reduced at 373 or 423 K were kept at 773 K under vacuum for 1 and 2 h, respectively, and then the same samples were oxidized at 673 K for 30 and 60 min. It has been shown that, on heating, Rh supported on CeO₂^{28,48} or other oxides tends to sinter.^{5,49,50} On heating, a significant XPS intensity decrease was detected for the 1–5% Rh/CeO₂ samples in the Rh 3d region (Figure 3A,C, Table 1).

During the experimental work leading to our previous paper, after reduction at 773 K, a significant decrease in the Rh 3d peak intensity was observed. It was proven by EDX measurement that the Rh content did not change during this process, and X-ray diffractometry revealed no interaction with CeO₂; therefore, sublimation or dissolution into the support cannot be responsible for these changes in XPS intensity.³³

Transmission electron microscopy revealed that the average particle size was similar on both samples after low-temperature reduction (2.3 ± 1.1 nm), thus the particle density must be different on the surface. After heating, the average particle diameter increased to 3.3 ± 2.0 nm for 5% Rh and 2.5 ± 0.9 nm for the 1% Rh/CeO₂ sample (Figure 4).

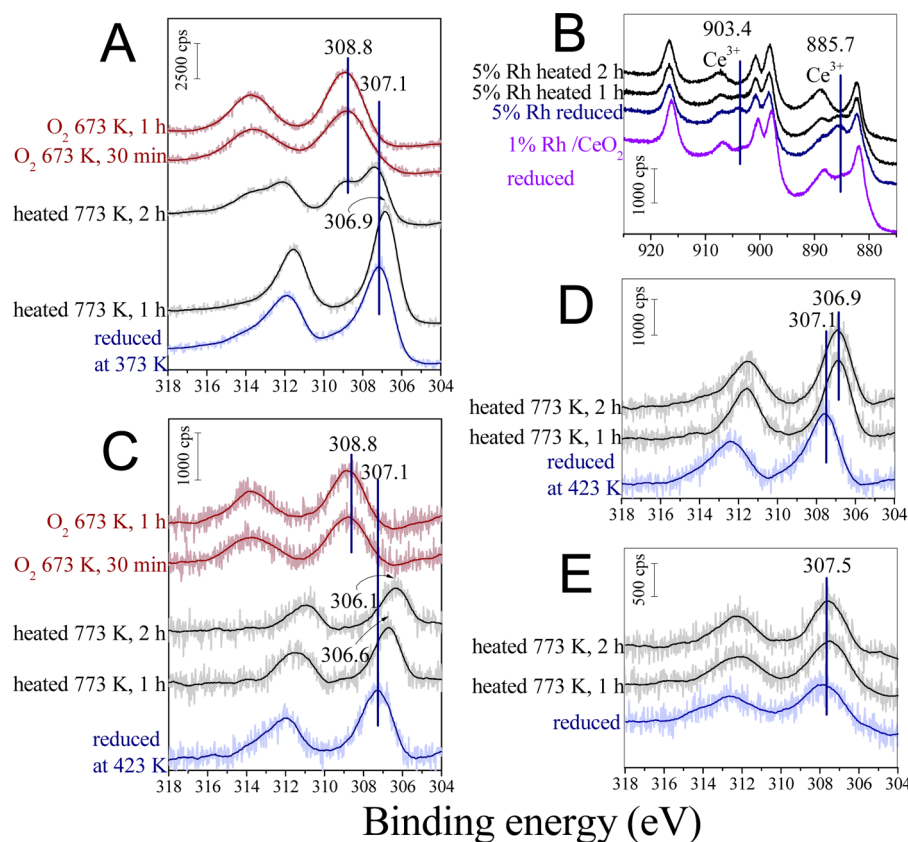


Figure 3. Rh 3d spectra of 5% Rh/CeO₂ (A), 1% Rh/CeO₂ (C), and 1% Rh + 2% Co/CeO₂ (D) after reduction, heating to 773 K in vacuum, and oxidation at 673 K as well as Ce 3d spectra of 5% Rh/CeO₂ (B). Comparative results on 1% Rh/Al₂O₃ (E).

Table 1. Relative Rh 3d Peak Areas (%)^a after Vacuum Agglomeration (after Reduction at Low Temperature) and Consecutive Reoxidation Experiments^b

sample	reduced in H ₂ at 773 K	in vacuo 773 K 1 h	in vacuo 773 K 2 h	O ₂ 673 K 30 min	O ₂ 673 K 1 h
5% Rh/CeO ₂	72	90	70	75	81
1% Rh/CeO ₂	48	61	48	63	74
1% Rh + 2% Co/CeO ₂	45	~100	~100		

^aPeak areas were referenced to the peaks obtained after low-temperature reduction: 15 min in H₂ at 673 K for 5% Rh/CeO₂ and 15 min in H₂ at 423 K for 1% Rh/CeO₂ and 1% Rh + 2% Co/CeO₂. ^bComparative results on high-temperature reduction (separate experiment) are in the first column.

In contrast, the relative XPS peak area changes included in Table 1 suggest a larger alteration for the 1% Rh/CeO₂ sample than for the one with 5% Rh. Because a wide range of Rh particle sizes were measured on the samples, it is worth paying attention to the particle size distributions (Figure 5). Here, it can be seen clearly that at high Rh content the sample became more heterogeneous: new, larger particles appeared, while for the 1% Rh/CeO₂ sample, the ratio of the smaller particles only decreased. This difference is attributed to the different particle numbers and the statistical growth of Rh. The coalescence of the very small metal particles could be the first step, which induces a more significant alteration in the surface area and intensity loss in XPS.

Not only the particle size increase but also, for reducible oxides such as CeO₂, the decoration effect can reduce the available surface.^{51,52} Here, this phenomenon plays only a

minor role because no intensity change in the CO vibrational region was detected even after high-temperature (773 K) reduction (Figure 2), similar to what was found by Bernal et al.⁵³ and in line with former results proving that decoration occurs only on Rh/CeO₂ reduced at temperature higher than 773 K.^{53–55}

Another interesting phenomenon is that the Rh 3d peak maximum shifted to lower values after heating at every Rh content. No relationship could be detected among the Rh 3d, Ce 3d, and O 1s spectra, which would unambiguously indicate bonding type changes. Unfortunately, this shift can be detected only for samples that had been stored under high vacuum, which makes a structural study by TEM impossible in our systems. However, for Au particles, some papers have already been published dealing with the separation of the initial and the final state effects in XPS. It was reported that the more spherical the particles are, the lower the average coordination number on the surface is, and the more dominant initial state effect causes the binding energy shift to lower values.^{56,57} In studies concerning Rh oxides, negative Rh 3d binding energy shifts were also ascribed to the metal–metal oxide interface.^{58,59} Because at this stage of experiment no Rh oxide was detected by XPS, a more relevant explanation could be the strong electronic interaction between the support and the supported metal playing an important role in heterogeneous catalysis.^{8,60,61} Sevcikova et al. also found a negative shift in the Rh 3d spectra of Rh supported on reduced CeO₂, having been attributed to the net negative charge on Rh resulting from Ce–Rh charge transfer.⁶² The contribution of this effect is also possible in this case.

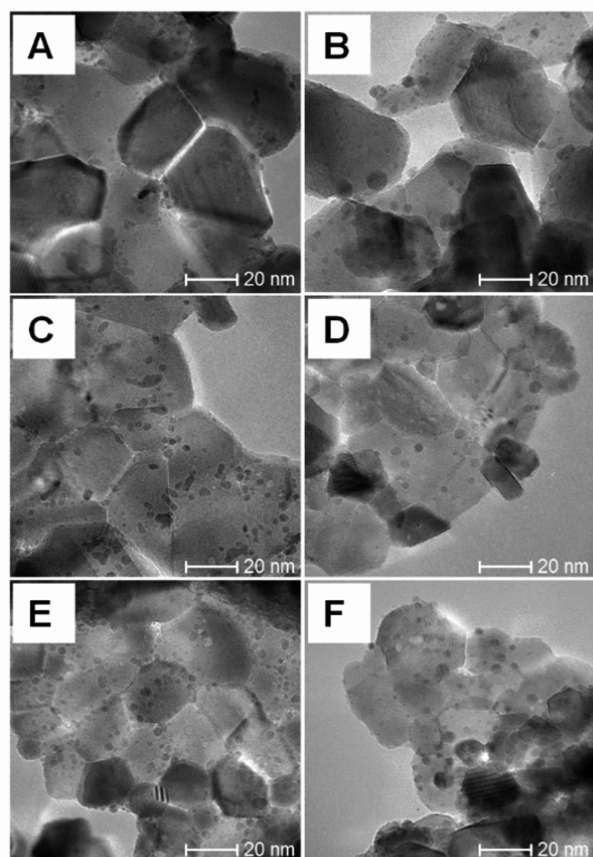


Figure 4. TEM images of 5% Rh/CeO₂ (A, B) 1% Rh/CeO₂ (C, D), and 2% Co + 1% Rh/CeO₂ (E, F) after low-temperature reduction and heat treatment, respectively. Rh particles appear as small, round dark spots on the significantly larger CeO₂ particles; Co is not discernible in panels E and F.

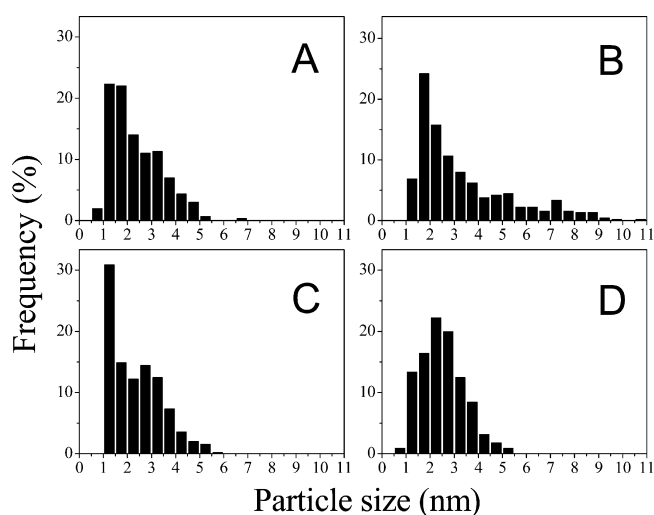


Figure 5. Rh particle size distributions of 5% Rh/CeO₂ after reduction (A) and 2 h of heating (B) and 1% Rh/CeO₂ after reduction (C) and heating (D).

For 1% Rh/CeO₂, trends similar to those for 5% Rh can be observed; however, the effects of both the agglomeration and redispersion were enhanced (Figure 3C, Table 1).

Bernal et al.⁵⁴ in their extended reduction and reoxidation HREM studies with Rh supported on low-surface-area CeO₂

(11 m²/g) reported similar observations that are included in the present work but in different temperature regimes. The Rh particle size started to increase at the 973 K reduction temperature, and this effect was significant at 1173 K. In addition, decoration by CeO₂ was observed over these two samples. Reoxidation up to 773 K did not result in changes in the Rh particle size; however, treatment at 1173 K induced smaller metal particles. This comparison points out the importance of the different experimental details (e.g., surface area and preparation methods); nevertheless, the general behavior of the systems is analogous.

Concerning Pd/Ce_{0.5}Zr_{0.5}O₂ catalysts, it was shown that the heat treatment in H₂ or N₂ induced the agglomeration of the precious metal; however, in the presence of O₂, this effect was hindered. When Pd was supported on Al₂O₃, a severe increase in particle size took place regardless of the aging atmosphere.⁶³ After calcination, the Pd/Ce_{0.5}Zr_{0.5}O₂ samples were treated with O₂-containing gas, and the redispersion of Pd particles was detected, which has a significant dependence on the cooling rate.⁶⁴ All of these observations were attributed to the probable formation of a Pd–O–Ce bond anchoring the Pd particles and inhibiting agglomeration. Similar effects were proposed for Au and Pt.^{65–67} As far as Rh is concerned, the presence of Rh–O–Ce bonding was detected in Rh/CeO₂/SiO₂ and Rh/CeO₂ samples by EXAFS.^{30,68}

Dictor et al. reported similar results on a CeO₂-doped Rh/Al₂O₃ sample.⁶⁹ In their work, FTIR spectroscopy was applied to characterize the morphology of Rh, while prolonged heating was applied to CO or H₂, resulting in the diminishing of dicarbonyl bands, indicating the agglomeration of Rh. After O₂ pulses at 673 K, the redispersion of the metal was observed. It was stated that the CeO₂-promoted sample was more resistant toward agglomeration than the unpromoted one. Nevertheless, in our separate experiment with 1% Rh/Al₂O₃, no Rh 3d intensity decrease took place after reduction (Figure 3E); however, in the reduced state, the total peak area was only half of the value at 1% Rh/CeO₂ (Figure 3C), suggesting larger particles. It is assumed that above a specified particle distribution sintering is not favored.

To underline the previous statement, comparative results are depicted in Figure S2 on 1% Rh/CeO₂ reduced at low or high temperatures. When reduced at 773 K (separate experiment), Rh gave a dramatically lower 3d peak intensity than after low-temperature reduction, predicting larger particle sizes resulting from the double effect of heat treatment and reducing conditions (Table 1, Figure S2). Similar results were obtained for the 5% Rh/CeO₂ sample. However, when 1% Rh/CeO₂ was linearly heated to 773 K in N₂ after high-temperature reduction, only one new component was detected at 308.8 eV as a result of oxygen spillover to Rh without any additional peak area changes. Here, it is intended to show that when extremely sintered Rh particles are heated under an inert atmosphere, additional aggregation hardly takes place. On the other hand, the oxygen spillover from CeO₂ is not enough to fully oxidize and disrupt the particles.

The addition of 2% Co changed the behavior of the sample completely; after heating, only a minor peak shift was observed without a decrease in the Rh 3d peak area (Figure 3D). Most particles had a diameter of between 1 and 1.5 nm (Figure 4), thus it can be concluded that Co inhibits the formation of large Rh particles. In the literature, the enrichment of the transition metal on the noble metal surface is also suggested.^{70,71} This could have an effect on the coalescence of Rh particles as well

as the alloy formation between Co and high Rh content. A behavior like this was identified for Rh/MgO by EXAFS and FTIR CO adsorption studies.^{71–73}

In our case, the total amount of Co is still in the oxidized state after the low-temperature reduction; therefore, alloy formation is not likely. In addition, referring to our previous results in which a wide range of Co–Rh samples with different Co–Rh contents were studied, the Rh 3d and Co 2p binding energies did not shift in the bimetallic samples compared to in the monometallic ones.³³ DRIFT spectra could not prove the formation of bimetallic particles either. Co dissolved into the support so strongly, as proven by the combination of XPS and low-energy ion scattering spectroscopy (LEIS), that it could not be studied by either XRD or TEM. On the basis of the lack of the strong electronic interaction and the similarity of the Rh particle sizes on 1% Rh/CeO₂ and 1% Rh + 2% Co/CeO₂, we suggest that Rh and the well-dispersed Co species (mainly Co²⁺) form separate phases. These objects must be close to each other because hydrogen spillover can take place. Co could inhibit the sintering of Rh by blocking its migration.

In Table 1 it is demonstrated that on heating in H₂, a comparable peak area decrease occurred over the 1% Rh + 2%/CeO₂ sample comparable to that after 2 h of heating in vacuum over the 1% Rh/CeO₂ sample, indicating the importance of the atmosphere. The dispersing effect of Co on Rh is still valid because the starting Rh 3d peak area is significant larger in the presence of Co, thus smaller particles must be considered at the beginning and, consequently, after sintering.

3.3. Effect of the CeO₂ Oxygens and the Reoxidation of Rhodium. In addition to the former observations concerning temperature-induced agglomeration, the partial oxidation of Rh at 5% during 2 h of heating was also detected. Taking into account the previous results with similar samples, this can be related to the enhanced O mobility of CeO₂ at high temperature.³³ The addition of more Rh resulted in a more intense reduction of CeO₂ (the Ce³⁺/(Ce³⁺ + Ce⁴⁺) ratio was 27% compared to 23% at 1% Rh, Figure S1), causing a steeper O gradient, which can enhance the segregation of O (Figure 3B). By the end of the 2 h long heating, the Ce³⁺ content decreased to 10%, similar to the value obtained after oxidation. A similar trend was observed over 1% Rh/CeO₂ and 1% Rh + 2% Co/CeO₂ but with much smaller spectral changes. On the other hand, the various reduction state of a reducible oxide can also influence the agglomeration process because O vacancies of the oxide support stabilize the dispersed state.^{74–77} However, the effect here is controversial because, according to some theoretical work, Rh does not tend to sit inside the vacancies;⁷⁸ moreover, subsurface vacancies are more stable than the ones in the topmost layer.⁷⁹

In some work, enhanced O-storage capacity by supercharging (presence of surface superoxide ions (O₂^{•−})) on the surface was concluded for small CeO₂ particles,^{80–82} while the photocatalytic activity of ceria was attributed to the formation of superoxide radicals.^{83,84} Significant changes in the O 1s region was observed only for high Rh content (Figure 6). The main peak centered at 529.3 eV is unambiguously identified as ceria lattice oxygen. Because the intensity of the smaller component at 531.2 eV was similar after oxidation and reduction, it is attributed to the presence of surface –OH groups rather than to vacancy-related species.^{82,85,86} Water (533.1 eV) was removed by heat treatment, and a new component emerged at 530.2 eV. Comparing it with our Rh 3d results, in which after 2 h of heating part of the Rh was oxidized and after oxidation

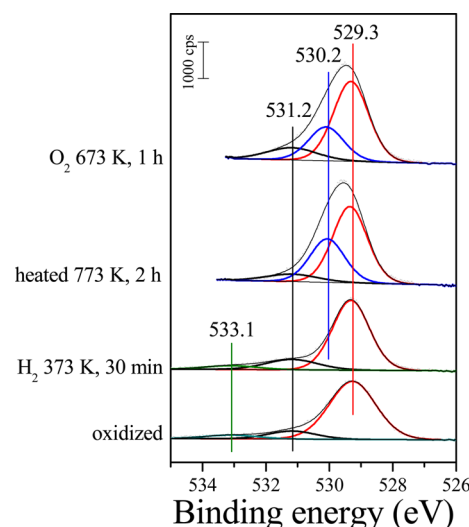


Figure 6. O 1s spectra of 5% Rh/CeO₂ after oxidation, total reduction, heating, and reoxidation.

Rh was in the oxidized state completely, we ascribe it to metal-bonded O and OH species on the surface of the Rh particles.^{87,88} The intensity discrepancy can be due to the different stoichiometry. After 2 h of heating, oxygen was deposited on top of the Rh particles, but during oxidation, Rh₂O₃ formation took place. Similar reverse O-spillover from CeO₂ to Pt was demonstrated by Vayssilov et al.⁸⁹ as well as by Zafiridis et al. for Rh/CeO₂.¹⁵ On Pt/CeO_x/TiO₂(110), Bruix et al. obtained the same effect.⁹⁰ Lin et al. demonstrated by ¹⁸O labeling that the oxygen in reoxidized PtO_x definitely originated from the ceria lattice instead of the O₂ reagent. They also emphasized the role of the surface OH group in the stabilization of dispersed particles.⁶⁷

When reoxidized in O₂ flow after agglomeration, in the 1–5% Rh/CeO₂ samples, the Rh 3d_{5/2} peak was located at 308.8 eV with a larger fwhm than after oxidation pretreatment at the beginning (Figures 1A,B and 3A,C). It is attributed to the formation of Rh₂O₃; nevertheless, the contribution of Rh-oxides with other stoichiometry cannot be excluded.^{58,91,92} In Figure 3A,C and Table 1, it is well demonstrated that the peak area also increased stepwise under oxidation. According to TEM measurements, most Rh particles had diameters in the 1–1.5 nm region.

As an additional experiment, we probed the temperature-induced agglomeration on the oxidized 1% Rh/CeO₂ sample and summarized the results in Figure 7. The supported metal was fully reduced after the first hour of heating, and similar Rh 3d peak area changes were obtained to that found on the reduced sample. On the other hand, CeO₂ exhibited opposite behavior compared to the previous observations in this work, and it was slightly reduced under heating. The increased number of O vacancies in CeO₂ on heating has been frequently presented.^{85,93} Considering that on the as-received sample and on the metal-free CeO₂ no changes took place (not shown), the release of O₂ molecules is assumed, which is catalyzed by Rh. Experimental and theoretical studies verify that the addition of noble metals enhances the reduction of CeO₂ as a result of the appearance of metal-induced gap states, which offer the opportunity to accommodate extra electrons.^{94–96}

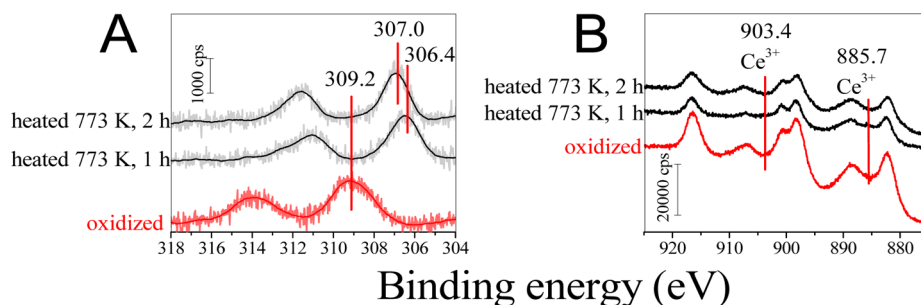


Figure 7. Rh 3d (A) and Ce 3d (B) spectra of 1% Rh/CeO₂ after oxidation and subsequent heating in vacuum.

4. SUMMARY AND CONCLUSIONS

The effects of metal loading and the Co additive on the temperature-induced agglomeration of Rh were studied in Rh/CeO₂ and Rh + Co/CeO₂ samples. Our conclusions are summarized as follows.

(1) XPS revealed that Rh supported on CeO₂ can be reduced at low temperature (at 373 K for 5% Rh and 423 K for 1% Rh content). The Rh 3d peak areas did not change until complete reduction. Carbon monoxide was adsorbed as gem-dicarbonyls over 1% Rh, and over 5% Rh, it was predominant as well. Thus, it was concluded that the Rh content can be reduced in the 373–423 K temperature range without the aggregation of the metal particles. TEM investigations proved that the average particle size was similar at 1–5% Rh loadings (~2.3 nm); however, the particle size distribution is heterogeneous.

(2) On the basis of the Rh 3d intensity decrease and TEM measurements a particle size increase was detected over the Rh/CeO₂ samples after heating in vacuum. From comparative studies with Rh/Al₂O₃ and Rh/CeO₂ reduced at 773 K, we suggest that at a given particle size distribution the agglomeration process is no longer favorable. Because no intensity decrease took place in the CO vibration region in our DRIFT experiment, we attribute only a minor role to the encapsulation of Rh by CeO₂. The addition of Co prohibited the sintering process when the sample was heated in vacuum.

(3) The oxygen treatments at elevated temperature (673 K) were able to redisperse the aggregated Rh particles, probably because of the formation of Ce–O–Rh bonds.

(4) XP spectra revealed that the mobile oxygens of CeO₂ fundamentally determine the oxidation state of the supported metals. At elevated temperature, the oxidation of the reduced support surface and the metals takes place because of the segregation of oxygen species originating from ceria at the surface. On the other hand, the oxidized CeO₂ surface can release oxygen easily in the presence of Rh accompanied by the reduction of the noble metal.

■ ASSOCIATED CONTENT

Supporting Information

The Supporting Information is available free of charge on the ACS Publications website at DOI: [10.1021/acs.langmuir.5b04482](https://doi.org/10.1021/acs.langmuir.5b04482).

Deconvoluted Ce 3d spectrum of 5% Rh/CeO₂ after low-temperature reduction and Rh 3d spectra of 1% Rh/CeO₂ (PDF)

■ AUTHOR INFORMATION

Corresponding Author

*E-mail: jkiss@chem.u-szeged.hu.

Notes

The authors declare no competing financial interest.

■ ACKNOWLEDGMENTS

This work was supported by the Alexander von Humboldt Foundation within the Research Group Linkage Program.

■ REFERENCES

- (1) Musselwhite, N.; Somorjai, G. A. Investigations of structure sensitivity in heterogeneous catalysis: From single crystals to monodisperse nanoparticles. *Top. Catal.* **2013**, *56*, 1277–1283.
- (2) Freund, H.-J.; Nilius, N.; Risse, T.; Schauermaier, S. A fresh look at an old nanotechnology: catalysis. *Phys. Chem. Chem. Phys.* **2014**, *16*, 8148–8167.
- (3) Goodman, D. W. Chemistry: Precious little catalyst. *Nature* **2008**, *454*, 948–949.
- (4) Park, J. Y.; Zhang, Y.; Grass, M.; Zhang, T.; Somorjai, G. A. Tuning of catalytic CO oxidation by changing composition of Rh–Pt nanoparticles. *Nano Lett.* **2008**, *8*, 673–677.
- (5) Berkó, A.; Solymosi, F. Adsorption-induced structural changes of Rh supported by TiO₂(110)-(1 × 2): An STM study. *J. Catal.* **1999**, *183*, 91–101.
- (6) Frank, M.; Kühnemuth, R.; Bäumer, M.; Freund, H.-J. Oxide-supported Rh particle structure probed with carbon monoxide. *Surf. Sci.* **1999**, *427–428*, 288–293.
- (7) Morgado, E., Jr.; de Abreu, M. A. S.; Moure, G. T.; Marinkovic, B. A.; Jardim, P. M.; Araujo, A. S. Effects of thermal treatment of nanostructured titanates on their crystallographic and textural properties. *Mater. Res. Bull.* **2007**, *42*, 1748–1760.
- (8) Pótári, G.; Madarász, D.; Nagy, L.; László, B.; Sági, A.; Oszkó, A.; Kukovecz, Á.; Erdőhelyi, A.; Kónya, Z.; Kiss, J. Rh-induced support transformation phenomena in titanate nanowire and nanotube catalysts. *Langmuir* **2013**, *29*, 3061–3072.
- (9) Iizuka, T.; Tanaka, Y.; Tanabe, K. Hydrogenation of CO and CO₂ over rhodium catalysts supported on various metal oxides. *J. Catal.* **1982**, *76*, 1–8.
- (10) Karelövic, A.; Ruiz, P. CO₂ hydrogenation at low temperature over Rh/γ-Al₂O₃ catalysts: Effect of the noble metal particle size on catalytic performances and reaction mechanism. *Appl. Catal., B* **2012**, *113–114*, 237–249.
- (11) Henderson, M. A. A surface science perspective in TiO₂ photocatalysis. *Surf. Sci. Rep.* **2011**, *66*, 185–297.
- (12) Watson, A. M.; Zhang, X.; de la Osa, R. A.; Sanz, J. M.; González, F.; Moreno, F.; Finkelstein, G.; Liu, J.; Everitt, H. O. Rhodium nanoparticles for ultraviolet plasmonics. *Nano Lett.* **2015**, *15*, 1095–1100.
- (13) Ola, O.; Maroto-Valer, M. M. Review of material design and reactor engineering on TiO₂ photocatalysis for CO₂ reduction. *J. Photochem. Photobiol., C* **2015**, *24*, 16–42.
- (14) Yao, H. C.; Yu Yao, Y. C. Ceria in automotive exhaust catalysts. I. Oxygen storage. *J. Catal.* **1984**, *86*, 254–265.
- (15) Zafiridis, G. S.; Gorte, R. J. Evidence for low-temperature oxygen migration from ceria to Rh. *J. Catal.* **1993**, *139*, 561–567.

- (16) Schlatter, J. C.; Mitchell, P. J. Three-way catalyst response to transients. *Ind. Eng. Chem. Prod. Res. Dev.* **1980**, *19*, 288–293.
- (17) Kim, G. Ceria-promoted three-way catalysts for auto exhaust emission control. *Ind. Eng. Chem. Prod. Res. Dev.* **1982**, *21*, 267–274.
- (18) da Silva, A. M.; de Souza, K. R.; Jacobs, G.; Graham, U. M.; Davis, B. H.; Mattos, L. V.; Noronha, F. V. Steam and CO₂ reforming of ethanol over Rh/CeO₂ catalyst. *Appl. Catal., B* **2011**, *102*, 94–109.
- (19) Sheng, P. Y.; Yee, A.; Bowmaker, G. A.; Idriss, H. H₂ Production from Ethanol over Rh–Pt/CeO₂ Catalysts: The Role of Rh for the Efficient Dissociation of the Carbon–Carbon Bond. *J. Catal.* **2002**, *208* (2), 393–403.
- (20) Sadi, F.; Duprez, D.; Gérard, F.; Miloudi, A. Hydrogen formation in the reaction of steam with Rh/CeO₂ catalysts: A tool for characterising reduced centers of ceria. *J. Catal.* **2003**, *213*, 226–234.
- (21) Ferencz, Z.; Erdőhelyi, A.; Baán, K.; Oszkó, A.; Óvári, L.; Kónya, Z.; Papp, C.; Steinrück, H. P.; Kiss, J. Effects of support and Rh additive on Co-based catalysts in the ethanol steam reforming reaction. *ACS Catal.* **2014**, *4*, 1205–1218.
- (22) Varga, E.; Ferencz, Z.; Oszkó, A.; Erdőhelyi, A.; Kiss, J. Oxidation states of active catalytic centers in ethanol steam reforming reaction on ceria based Rh doped Co catalysts: An XPS study. *J. Mol. Catal. A: Chem.* **2015**, *397*, 127–133.
- (23) Mattos, L. V.; Jacobs, G.; Davis, B. H.; Noronha, F. B. Production of Hydrogen from Ethanol: Review of reaction mechanism and catalyst deactivation. *Chem. Rev.* **2012**, *112*, 4094–4123.
- (24) Mukainakano, Y.; Li, B.; Kado, S.; Miyazawa, T.; Okumura, K.; Miyao, T.; Naito, S.; Kunimori, K.; Tomishige, K. Surface modification of Ni catalysts with trace Pd and Rh for oxidative steam reforming of methane. *Appl. Catal., A* **2007**, *318*, 252–264.
- (25) Kiennemann, A.; Breault, R.; Hindermann, J. P. Ethanol promotion by the addition of cerium to rhodium-silica catalysts. *J. Chem. Soc., Faraday Trans. 1* **1987**, *83*, 2119–2128.
- (26) Zafir, G. S.; Gorte, R. J. Evidence for a second CO oxidation mechanism on Rh/ceria. *J. Catal.* **1993**, *143*, 86–91.
- (27) Cordatos, H.; Bunluesin, T.; Stubenrauch, J.; Vohs, M.; Gorte, R. J. Effect of ceria structure on oxygen migration for Rh/ceria catalysts. *J. Phys. Chem.* **1996**, *100*, 785–789.
- (28) Overbury, S. H.; Mullins, D. R.; Kundakovic, L. Enhancement of dissociation by metal-support interaction: reaction of NO on Rh supported by ceria films of controlled oxidation state. *Surf. Sci.* **2001**, *470*, 243–254.
- (29) Zhou, J.; Baddorf, A. P.; Mullins, D. R.; Overbury, S. H. Growth and characterization of Rh and Pd nanoparticles on oxidized and reduced CeO_x(111) thin films by scanning tunneling microscopy. *J. Phys. Chem. C* **2008**, *112*, 9336–9345.
- (30) Miyazawa, T.; Okumura, K.; Kunimori, K.; Tomishige, K. Promotion of oxidation and reduction of Rh species by interaction of Rh and CeO₂ over Rh/CeO₂/SiO₂. *J. Phys. Chem. C* **2008**, *112*, 2574–2583.
- (31) Trovarelli, A.; Fomasiero, P. *Catalysis by Ceria and Related Materials*, 2nd ed.; Imperial College Press: London, 2013; p 888.
- (32) Campbell, C. T.; Peden, C. H. I. Oxygen vacancies and catalysis on ceria surfaces. *Science* **2005**, *309*, 713–714.
- (33) Varga, E.; Pusztai, P.; Óvári, L.; Oszkó, A.; Erdőhelyi, A.; Papp, C.; Steinrück, H.-P.; Kónya, Z.; Kiss, J. Probing the interaction of Co, Rh and Co-Rh bimetallic particles with the CeO₂ support: catalytic materials for alternative energy generation. *Phys. Chem. Chem. Phys.* **2015**, *17*, 27154–27166.
- (34) Burroughs, P.; Hamnett, A.; Orchard, A. F.; Thornton, G. Satellite structure in the X-ray photoelectron spectra of some binary and mixed oxides of lanthanum and cerium. *J. Chem. Soc., Dalton Trans.* **1976**, *17*, 1686–1698.
- (35) Zhang, J.; Yu, X.; Wu, Z. Y.; Liu, T.; Hu, T. D.; Xie, Y. N. Structural characteristics of cerium oxide nanocrystals prepared by the microemulsion method. *Chem. Mater.* **2001**, *13*, 4192–4197.
- (36) Fouad, N. E.; Mohamed, M. A.; Zaki, M. I.; Knözinger, H. Thermal and spectroscopic studies of feasibility of rhodium acetate versus chloride as a likely precursor for Rh metal catalysts. *J. Anal. Appl. Pyrolysis* **2000**, *53*, 185–193.
- (37) Munuera, G.; Gonzales-Elipe, A. R.; Espinos, J. P.; Munos, A.; Conesa, J. C.; Soria, J.; Sanz, J. The role of oxygen vacancies during the decomposition of RhCl₃/TiO₂ precursor: Study by XPS, IR, EPR and NMR. *Catal. Today* **1988**, *2*, 663–673.
- (38) Kondarides, D.; Verykios, X. The effect of chlorine on the chemisorptive properties of Rh/CeO₂ catalysts studied by XPS and temperature programmed desorption techniques. *J. Catal.* **1998**, *174*, 52–64.
- (39) Pereira, E. B.; Homes, N.; Martí, S.; Fierro, J. L. G. Oxidative steam-reforming of ethanol over Co/SiO₂, Co–Rh/SiO₂ and Co–Ru/SiO₂ catalysts: Catalytic behavior and deactivation/regeneration processes. *J. Catal.* **2008**, *257*, 206–214.
- (40) van't Blik, H. F. J.; Koningsberger, D. C.; Prins, R. Characterization of supported cobalt and cobalt-rhodium catalysts: III. Temperature programmed Reduction (TPR), oxidation (TPO), and EXAFS of Co-Rh/SiO₂. *J. Catal.* **1986**, *97*, 210–218.
- (41) Ligthart, D. A. J. M.; van Santen, R. A.; Hensen, E. J. M. Influence of particle size on the activity and stability in steam methane reforming of supported Rh nanoparticles. *J. Catal.* **2011**, *280*, 206–220.
- (42) Underwood, R. P.; Bell, A. T. Lanthana-promoted Rh/SiO₂. *J. Catal.* **1988**, *109*, 61–75.
- (43) Mo, X.; Gao, J.; Umnajaseam, N.; Goodwin, J. G. J. La, V, and Fe promotion of Rh/SiO₂ for CO hydrogenation: Effect on adsorption and reaction. *J. Catal.* **2009**, *267*, 167–176.
- (44) Solymosi, F.; Pásztor, M. *J. Phys. Chem.* **1985**, *89*, 4789–4793.
- (45) Van't Blik, H. F. J.; Van Zon, J. B. A. D.; Hulzinga, T.; Vis, J. C.; Koningsberger, D. C.; Prins, R. An extended X-ray absorption fine structure spectroscopy study of a highly dispersed Rh/Al₂O₃ catalyst: The influence of CO chemisorption on the topology of rhodium. *J. Phys. Chem.* **1983**, *87*, 2264–2267.
- (46) Bulushev, D. A.; Froment, G. F. A DRIFTS study of the stability and reactivity of adsorbed CO species on a Rh/γ-Al₂O₃ catalyst with a very low metal content. *J. Mol. Catal. A: Chem.* **1999**, *139*, 63–72.
- (47) Rice, C. A.; Worley, S. D.; Curtis, C. W.; Guin, J. A.; Tarrer, A. R. The oxidation state of dispersed Rh on Al₂O₃. *J. Chem. Phys.* **1981**, *74*, 6487–6497.
- (48) Stubenrauch, J.; Vohs, J. M. Interaction of CO with Rh supported on stoichiometric and reduced CeO₂(111) and CeO₂(100) surfaces. *J. Catal.* **1996**, *159*, 50–57.
- (49) Ozturk, O.; Park, J. B.; Ma, S.; Ratliff, J. S.; J, Z.; Mullins, D. R.; Chen, D. A. Probing the interactions of Pt, Rh and bimetallic Pt-Rh clusters with the TiO₂(110) support. *Surf. Sci.* **2007**, *601*, 3099–3113.
- (50) Óvári, L.; Kiss, J. Growth of Rh nanoclusters on TiO₂(110): XPS and LEIS studies. *Appl. Surf. Sci.* **2006**, *252*, 8624–8629.
- (51) Sun, H. P.; Pan, X. P. Partial encapsulation of Pd particles by reduced ceria-zirconia. *Appl. Phys. Lett.* **2005**, *87*, 201915.
- (52) Caballero, A.; Holgado, J. P.; Gonzales-de la Cruz, V. M.; Habas, S. E.; Herranz, T.; Salmeron, H. In situ spectroscopic detection of SMSI effect in a Ni/CeO₂ system: hydrogen induced burial and dig out of metallic nickel. *Chem. Commun.* **2010**, *46*, 1097–1099.
- (53) Bernal, S.; Botana, F. J.; Calvino, J. J.; Cauqui, M. A.; Cifredo, G. A.; Jobacho, A.; Pintado, J. M.; Rodríguez-Isquierdo, J. M. Microstructural and chemical properties of ceria-supported rhodium catalysts reduced at 773 K. *J. Phys. Chem.* **1993**, *97*, 4118–4123.
- (54) Bernal, S.; Botana, F. J.; Calvino, J. J.; Cifredo, G. A.; Pérez-Omil, J. A.; Pintado, J. M. HREM study of the behaviour of a Rh/CeO₂ catalyst under high temperature reducing and oxidizing conditions. *Catal. Today* **1995**, *23*, 219–250.
- (55) Bernal, S.; Calvino, J. J.; Cauqui, M. A.; Cifredo, G. A.; Jobacho, A.; Rodríguez-Isquierdo, J. M. Metal-support interaction phenomena on rhodium/ceria and rhodium/titania catalysts: Comparative study by high-resolution transmission electron spectroscopy. *Appl. Catal., A* **1993**, *99*, 1–8.
- (56) Radnik, J.; Mohr, C.; Claus, P. On the origin of binding energy shifts of core levels of supported gold nanoparticles and dependence of pretreatment and material synthesis. *Phys. Chem. Chem. Phys.* **2003**, *5*, 172–177.

- (57) Costanzo, E.; Faraci, G.; Pennisi, A. R.; Ravesi, S.; Terrasi, A. Initial and final state effects in photoemission from gold clusters. *Solid State Commun.* **1992**, *81*, 155–158.
- (58) Gustafson, J.; Westerström, R.; Resta, A.; Mikkelsen, A.; Andersen, J. N.; Balmes, O.; Torrelles, X.; Schmid, M.; P, V.; Hammer, B.; Kresse, G.; Baddeley, C. J.; Lundgren, E. Structure and catalytic reactivity of Rh oxides. *Catal. Today* **2009**, *145*, 227–235.
- (59) Zhan, R. R.; Vesselli, E.; Baraldi, A.; Lizzit, S.; Comelli, G. The Rh oxide ultrathin film on Rh(110): An X-ray photoelectron diffraction study. *J. Chem. Phys.* **2010**, *133*, 214701.
- (60) Solymosi, F. Importance of the electric properties of supports in the carrier effect. *Catal. Rev.: Sci. Eng.* **1968**, *1*, 233–255.
- (61) Sasahara, A.; Pang, C. L.; Onishi, H. Probe microscope observation of platinum atoms deposited on the $\text{TiO}_2(110)-(1 \times 1)$ surface. *J. Phys. Chem. B* **2006**, *110*, 13453–13457.
- (62) Sevcikova, K.; Kolarova, T.; Skala, T.; Tsud, N.; Vaclav, M.; Lykhach, Y.; Matolin, V.; Nehasil, V. Impact of Rh-CeO_x interaction on CO oxidation mechanism. *Appl. Surf. Sci.* **2015**, *332*, 747–755.
- (63) Cao, Y.; Ran, R.; Wu, X.; Zhao, B.; Wan, J.; Weng, D. Comparative study of ageing conditions effects on Pd/Ce_{0.5}Zr_{0.5}O₂ and Pd/Al₂O₃ catalysts: Catalytic activity, palladium nanoparticle structure and Pd-support interaction. *Appl. Catal., A* **2013**, *457*, 52–61.
- (64) Wan, J.; Ran, R.; Wu, X.; Cao, Y.; Li, M.; Weng, D. Re-dispersion of Pd on Ce_{0.5}Zr_{0.5}O₂ upon cooling in the presence of oxygen. *Catal. Today* **2015**, *253*, 51–56.
- (65) Nagai, Y.; Dohmae, K.; Ikeda, Y.; Takagi, N.; Hara, N.; Tanabe, T.; Guiler, G.; Pascarelli, S.; Newton, M. A.; Takahashi, N.; Shinjoh, H.; Matsumoto, S. In situ observation of platinum sintering on ceria-based oxide for autoexhaust catalysts using Turbo-XAS. *Catal. Today* **2011**, *175*, 133–140.
- (66) Fu, Q.; Saltsburg, H.; Flytzani-Stephanopoulos, M. Active nonmetallic Au and Pt species on ceria-based water-gas shift catalysts. *Science* **2003**, *301*, 935–938.
- (67) Lin, W.; Herzing, A. A.; Kiely, C. J.; Wachs, I. E. Probing metal-support interactions under oxidizing and reducing conditions: In situ Raman and infrared spectroscopic and scanning transmission electron microscopic - X-ray energy-dispersive spectroscopic investigation of supported platinum catalysts. *J. Phys. Chem. C* **2008**, *112*, 5942–5951.
- (68) Hosokawa, S.; Taniguchi, M.; Utani, K.; Kanai, H.; Imamura, S. Affinity order among noble metals and CeO₂. *Appl. Catal., A* **2005**, *289*, 115–120.
- (69) Dictor, R.; Roberts, S. Influence of ceria on alumina-supported rhodium; observations of rhodium morphology made using FTIR spectroscopy. *J. Phys. Chem.* **1989**, *93*, 5846–5850.
- (70) Wang, Z.; Yang, F.; Axnanda, S.; Liu, C.; Goodman, D. W. Preparation and characterization of Co-Rh bimetallic model catalysts: From thin films to dispersed clusters. *Appl. Catal., A* **2011**, *391*, 342–349.
- (71) Tanaka, H.; Kaino, R.; Okumura, K.; Kizuka, T.; Nakagawa, Y.; Tomoshige, K. Comparative study of Rh/MgO with Fe, Co or Ni for the catalytic partial oxidation of methane at short contact time. Part I. Characterization of catalysts. *Appl. Catal., A* **2010**, *378*, 175–186.
- (72) Naito, S.; Tanaka, H.; Kado, S.; Toshihiro, M.; Naito, S.; Okumura, K.; Kunitomi, K.; Tomoshige, K. Promoting effect of Co addition on the catalytic partial oxidation of methane at short contact time over a Rh/MgO catalyst. *J. Catal.* **2008**, *259*, 138–146.
- (73) Li, D.; Sakai, S.; Nakagawa, Y.; Tomoshige, K. FTIR study of CO adsorption on Rh/MgO modified with Co, Ni, Fe or CeO₂ for the catalytic partial oxidation of methane. *Phys. Chem. Chem. Phys.* **2012**, *14*, 9204–9213.
- (74) Kim, Y. D.; Stultz, J.; Wei, T.; Goodman, D. W. Interaction of Ag with MgO(110). *J. Phys. Chem. B* **2002**, *106*, 6827–6830.
- (75) Zhang, C.; Michaelides, A.; King, D. A.; Jenkins, S. J. Anchoring sites for initial Au nucleation in CeO₂{111}: O vacancy versus Ce vacancy. *J. Phys. Chem. C* **2009**, *113*, 6411–6417.
- (76) Sanchez, M. G.; Gazquez, J. L. Oxygen vacancy model in strong metal-support interaction. *J. Catal.* **1987**, *104*, 120–135.
- (77) Pusztai, P.; Puskás, R.; Varga, E.; Erdőhelyi, A.; Kukovecz, Á.; Kónya, Z.; Kiss, J. The effect of gold additives on the stability and phase transformation of titanate nanostructures. *Phys. Chem. Chem. Phys.* **2014**, *16*, 26786–26797.
- (78) Lu, Z.; Yang, Z.; Hermansson, K.; Castleton, C. W. M. Several different charge transfer and Ce³⁺ localization scenarios for Rh-CeO₂(111). *J. Mater. Chem. A* **2014**, *2*, 2333–2345.
- (79) Murgida, G. E.; Ganduglia-Pirovano, M. V. Evidence for subsurface ordering of oxygen vacancies on the reduced CeO₂(111) subsurface using density-functional and statistical calculations. *Phys. Rev. Lett.* **2013**, *110*, 246101.
- (80) Kullgren, J.; Hermansson, K.; Broqvist, P. Supercharged low-temperature oxygen storage capacity of ceria at the nanoscale. *J. Phys. Chem. Lett.* **2013**, *4*, 604–608.
- (81) Renuka, N. K.; Harsha, N.; Divya, T. Supercharged ceria quantum dots with exceptionally high oxygen buffer action. *RSC Adv.* **2015**, *5*, 38837–38841.
- (82) Xu, J.; Harmer, J.; Li, G.; Chapman, T.; Collier, P.; Longworth, S.; Tsang, S. C. Size dependent oxygen buffering capacity of ceria nanocrystals. *Chem. Commun.* **2010**, *46*, 1887–1889.
- (83) Verma, R.; Samdarshi, S. K.; Bojja, S.; Paul, S.; Choudhury, B. A novel thermocatalyst of mixed-phase cerium oxide (CeO₂/Ce₂O₃) homocomposite nanostructure: Role of interface and oxygen vacancies. *Sol. Energy Mater. Sol. Cells* **2015**, *141*, 414–422.
- (84) Aslam, M.; Oamar, M. T.; Soomro, M. T.; Ismail, I. M. I.; Salah, N.; Almeelbi, T.; Gondal, M. A.; Hameed, A. The effect of sunlight induced surface defects on the photocatalytic activity of nanosized CeO₂ for the degradation of phenol its derivatives. *Appl. Catal., B* **2016**, *180*, 391–402.
- (85) Wang, K.; Chang, Y.; Lv, L.; Long, Y. Effect of annealing temperature on oxygen vacancy concentrations of nanocrystalline CeO₂ film. *Appl. Surf. Sci.* **2015**, *351*, 164–168.
- (86) Pereira, A.; Blouin, B.; Pillonnet, A.; Guay, D. Structure and valence properties of ceria films synthesized by laser ablation under reducing atmosphere. *Mater. Res. Express* **2014**, *1*, 015704.
- (87) Fierro, J. L. G.; Palacios, J. M.; Tomas, F. An analytical SEM and XPS study of platinum-rhodium gauzes used in high pressure ammonia burners. *Surf. Interface Anal.* **1988**, *13*, 25–32.
- (88) Blomberg, S.; Lundgren, E.; Westerström, R.; Erdogan, E.; Martin, N. M.; Mikkelsen, A.; Andersen, J. N.; Mittendorfer, F.; Gustafson, J. Structure of the Rh₂O₃(0001) surface. *Surf. Sci.* **2012**, *606*, 1416–1421.
- (89) Vayssilov, G. N.; Lykhach, Y.; Migani, A.; Staudt, T.; Petrova, G. P.; Tsud, N.; Skála, T.; Bruix, F.; Illas, F.; Prince, K. C.; Matolin, V.; Neyman, K. M.; Libuda, J. Support nanostructure boosts oxygen transfer to catalytically active platinum nanoparticles. *Nat. Mater.* **2011**, *10*, 310–315.
- (90) Bruix, A.; Rodriguez, J. A.; Ramirez, P. J.; Senanayake, S. D.; Evans, J.; Park, J. B.; Stacchiola, D.; Liu, P.; Hrbek, J.; Illas, F. A new type of strong metal-support interaction and the production of H₂ through the transformation of water on Pt/CeO₂(111) and Pt/CeO_x/TiO₂(110) catalysts. *J. Am. Chem. Soc.* **2012**, *134*, 8968–8974.
- (91) Nefedov, V. I.; Firsov, M. N.; Shaplygin, I. S. Electronic structures of MRhO₂, MRh₂O₄, RhMO₄ and Rh₂MO₆ on the basis of X-ray spectroscopy and ESCA data. *J. Electron Spectrosc. Relat. Phenom.* **1982**, *26*, 65–78.
- (92) Tolia, A. A.; Smiley, R. J.; Delgass, W. N.; Takoudis, C. G.; Weaker, M. J. Surface oxidation of rhodium at ambient pressures as probed by surface-enhanced Raman and X-ray photoelectron spectroscopies. *J. Catal.* **1994**, *150*, 56–70.
- (93) Nörenberg, H.; Briggs, G. A. D. Defect formation on CeO₂(111) surfaces after annealing studied by STM. *Surf. Sci.* **1999**, *424*, L352–L355.
- (94) Norman, A.; Perrichon, V.; Bensaddik, A.; Lemaux, S.; Bitter, H.; Koningsberger, D. Study of the reducibility of Pt or Pd on ceria-zirconia catalysts by XANES measured at the Ce L_{III} edge and magnetic susceptibility measurements. *Top. Catal.* **2001**, *16*, 363–368.

(95) Divins, N. J.; Llorca, J. In situ photoelectron spectroscopy study of ethanol steam reforming over RhPd nanoparticles and RhPd/CeO₂. *Appl. Catal., A* **2015**, DOI: [10.1016/j.apcata.2015.08.018](https://doi.org/10.1016/j.apcata.2015.08.018).

(96) Yang, Z.; Luo, G.; Lu, Z.; Woo, T. K.; Hermansson, K. Structural and electronic properties of NM-doped ceria (NM = Pt, Rh): a first-principle study. *J. Phys.: Condens. Matter* **2008**, *20*, 035210.